

Cite this: *Soft Matter*, 2012, **8**, 303

www.rsc.org/softmatter

COMMUNICATION

Ultimate strength of a colloidal packing

Arijit Sarkar and Mahesh S. Tirumkudulu

Received 12th September 2011, Accepted 2nd November 2011

DOI: 10.1039/c1sm06720f

The phenomenon of cracking in drying colloidal dispersions is investigated with a focus on the role of flaws on the critical stress required to nucleate cracks. Experiments show that the stress required to fracture a cylindrical colloidal packing saturated with solvent under axial tension varies inversely with the three-half powers of the diameter. The predicted critical stress required to initiate cracks from flaws shows the same scaling with flaw size. Close inspection of the failed sections of the packing revealed flaws entrapped during the drying process. The maximum capillary pressure sets the critical flaw size below which the crack will not nucleate, thereby giving the ultimate strength of the colloidal packing. The experiments show that if the flaw size can be restricted below the critical value, large colloidal packings free of cracks can be synthesized.

Understanding why and how cracks nucleate and spread in drying colloidal dispersions is important in describing naturally occurring processes such as cracking of soil and river beds along with many technological process applications such as paints and coatings, electronics, and pharmaceuticals.^{1,2} The colloidal dispersions normally consist of a particulate phase made of metal oxides³ or polymeric particles⁴ dispersed in a solvent which is either a low molecular weight solvent or more often water. During drying, particles concentrate until they come in contact and the menisci between the top layer of the particles formed by the liquid-air interface exerts capillary pressure on the packing. If the bed is constrained from shrinking, tensile stresses develop that can nucleate cracks when the stresses exceed a critical value. Many studies have investigated the conditions under which drying colloidal beds crack with focus on the thin film geometry.^{3–5} These studies have measured the critical stress at which a given film cracks and compared it with the stress required to drive an infinitely long crack through the film. The measured critical stresses were higher than the predicted value though the measured scaling of critical stress on the film thickness agrees well with the prediction. It is only recently that the role of pre-existing flaws in nucleating cracks have been highlighted by Russel and co-workers^{6,7} who attribute the discrepancy to the presence of such flaws.

The calculation of the critical cracking stress in stressed colloidal packings mirrors those first pioneered by Griffith⁸ almost a century ago who showed that the a pre-existing flaw in a brittle material will

expand into a crack when the elastic energy released due to stress relaxation in the material becomes equal to the increase in surface energy due to increase in crack length. These calculations utilized the stress field obtained by Inglis⁹ who showed that for a plate under a uniform far field stress and containing a flaw in the shape of an ellipse, the ratio of the stress at the corner of the elliptical hole to the far-field stress scales as $\sqrt{a/\rho}$ where a is the semi-major axis of the hole and ρ is the radius of curvature at the crack tip. Consequently, tiny flaws tend to concentrate stresses at the crack tip thereby reducing the strength of the material. Applying the aforementioned energy balance, the critical stress for cracking scaled as, $\sigma_c a^{1/2} \sim (E\gamma)^{1/2}$, where E is the modulus of the brittle material and γ is the interfacial tension. For experimental confirmation, Griffith measured the tensile strength required to break glass fibers and found that the fracture stress increased as the fiber diameter decreased, thereby suggesting that thinner fibers accommodate smaller flaws and so break at higher stresses. Thus the Griffith's criterion demonstrated that the uniaxial tensile strength could not be a specimen-independent material property and helped resolve the long standing difference between the relatively low stress needed to fracture brittle materials compared to the much higher theoretical stress values needed for breaking atomic bonds.

The question then arises if a similar experimental validation of the influence of flaws on the strength of a colloidal packing saturated with a solvent is possible. Specifically, is it possible to produce fibers of varying diameters made of a solvent-saturated packing of colloidal particles whose tensile strength can then be tested as a function of its diameter? In this work, we present novel experiments that measure the critical tensile stress required to break a thin colloidal bridge or "fiber" and show that the critical stress scales inversely with the fiber diameter. Packing faults and voids formed during the drying process act as flaws and are responsible for initiating the failure. Unlike brittle materials, there exists a critical diameter below which the fiber will not break which is set by the maximum possible capillary pressure that ultimately determines its strength.

Aqueous colloidal dispersion were prepared from alumina particles of mean diameter, $2R = 340$ nm (Sumitomo AKP-30[®]) at 5.1 pH and initial particle volume fraction, 0.53.¹⁰ The particles were monodisperse (PDI ~ 0.2) though not spherical. A small volume (50–100 μ l) of the dispersion was sandwiched between two parallel circular plates of a rheometer (MCP-301, Anton-Paar[®]) and allowed to dry (Fig. 1). The dispersion wetted only a small circular central section of the stationary plates. The wet dispersion forms a liquid bridge connecting the two plates, with the diameter of the thinnest (central)

Department of Chemical Engineering, Indian Institute of Technology Bombay, Powai, Mumbai, 400076, India

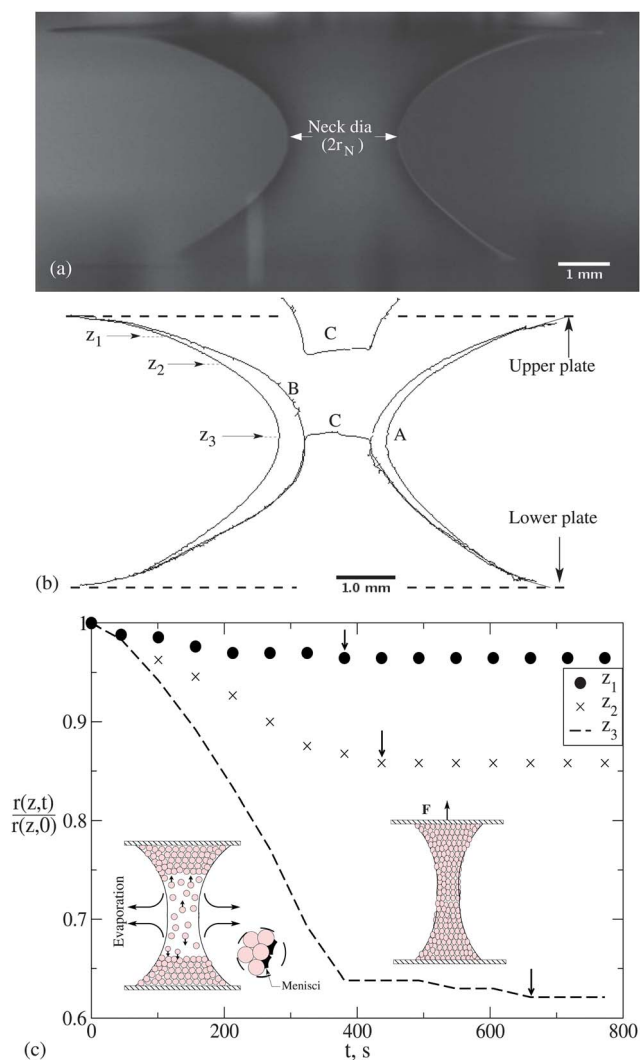


Fig. 1 (a) Image of the liquid bridge of colloidal dispersion drying between the plates of the rheometer. (b) The contours of the “fiber” are plotted at three different times. The corresponding force measurements are given in Fig. 2. (c) The average radius at three different vertical sections ($z = z_1, z_2, z_3$) are plotted as a function of time. A schematic of the drying mechanism is included. The capillary menisci between the particles is highlighted. The tensile force, F , is recorded by the force transducer connected to the top plate.

section of the liquid bridge controlled by either varying the volume of the dispersion or by varying the gap between the plates (Fig. 1(a)). Since the gaps are small (less than 5 mm), the shape of the liquid bridge is only slightly effected by gravity and it appears symmetric about the central horizontal section.

The particles pack first at the free surface especially at the edges of the film in contact with the top and bottom plates, and the capillary suction created by the menisci between the packed particles draws the particles and fluid from the central section of the liquid bridge. Consequently, a front separating the packed bed from the dilute dispersion region grows from either of the plates towards the central section of the liquid bridge, as indicated by the change in the radius at three different locations (Fig. 1(c)). The vertical arrows indicate the time after which the radius did not change. The time evolution of the shape of the liquid bridge (Fig. 1(b,c)) shows that the diameter of

the fiber at the center (neck) decreases the most compared to other sections of the bridge. Further, the fiber becomes slightly asymmetric once the particles completely pack. The contours A and B (Fig. 1(b)) correspond to the initial liquid bridge at the start of the experiment and when the fiber cracks, respectively. The contour C was obtained when the top plate was lifted which clearly shows that the fiber cracked at the neck.

A force sensor connected to the top plate measures the tensile force during this entire process. The force measurement presented in Fig. 2 corresponds to the experiment whose images are presented in Fig. 1(b). The measured force is negligible for $t < 600$ s suggesting that the particles have not completely packed and fluid connects parts of the liquid bridge. Once the entire liquid bridge transforms into a colloidal particle packing, the negative pressure of the liquid menisci pulls on the plates generating a tensile force. This arises because the fiber is free to contract in the radial direction while it is constrained in the vertical direction by the plates. In Fig. 2, the tensile force rises beyond $t \sim 650$ s reaching a maximum value at around 800 s, after which the force falls sharply to a negligible value. At the end of the experiment, the two plates were separated to determine the region where the fiber had cracked (contour C in Fig. 1(b)). In almost all cases, the fiber cracks at the neck where the diameter is the smallest. For the remaining experiments, the fiber de-bonded from one of the rheometer plates. The latter corresponded typically to those experiments where the neck diameter was very small. In many cases, the failed section showed the presence of hemispherical pockets suggesting that voids, trapped due to packing fronts advancing from different sides, may be responsible for initiating the failure (Fig. 2, inset).

While the experiments performed with the low pH alumina dispersion ($\sim \text{pH } 5.1$) were successful, those performed at higher pH values ($\text{pH} > 7$) did not generate any force and the samples debonded from the rheometer plates. This is because alumina is soluble at low pH which leads to redeposition of alumina from the particle surfaces to the particle contacts during drying.^{3,10} Consequently, the particle network is toughened and can withstand large stresses.

The critical stress for cracking is calculated by dividing the maximum force by the cross-sectional area of the neck. Fig. 3(a)

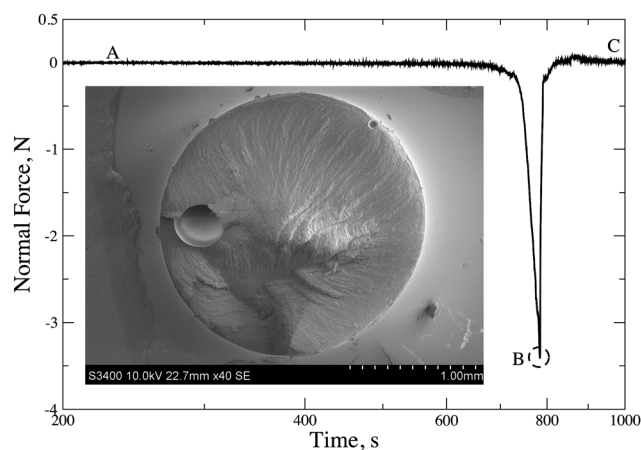


Fig. 2 Typical tensile force (negative) output from the rheometer. The three points (A–C) correspond to the images in Fig. 1(b). The inset presents the SEM image of the cross-section of a typical failed section with one large void left of center.

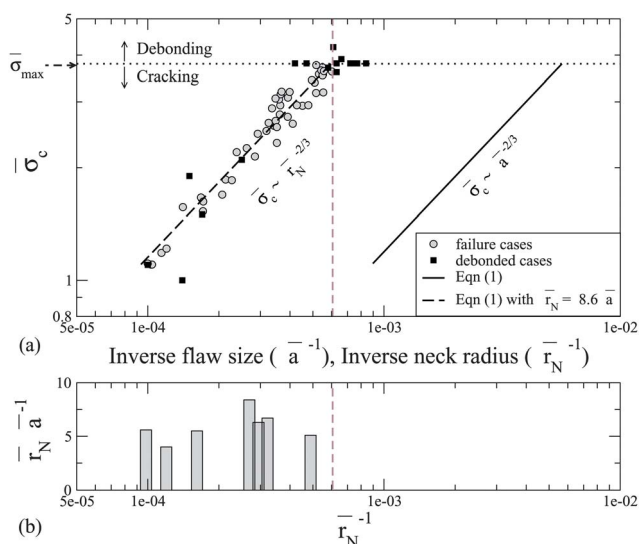


Fig. 3 (a) The measured (dimensionless) stress at the neck is plotted as a function of the dimensionless inverse neck radius (\bar{r}_N^{-1}). The solid line plots the predicted stress (1) as a function of dimensionless inverse flaw size (\bar{a}^{-1}). The dashed line was obtained by setting $\bar{r}_N = 8.6\bar{a}$ in (1). Here, $G = 156 \text{ GPa}$,¹³ $\gamma_{lg} = 0.072 \text{ Nm}^{-1}$, $\gamma_{sg} = 1.06 \text{ Nm}^{-1}$,¹⁴ $R = 170 \text{ nm}$, $\phi_{rcp} = 0.64^{10}$ and $M = 6$.¹⁰ (b) The ratio of neck to flaw radius is plotted against the dimensionless inverse neck radius.

presents the variation of the dimensionless critical stress ($\bar{\sigma}_c \equiv \sigma_c R / 2\gamma_{lg}$) as a function of the dimensionless inverse neck radius ($\bar{r}_N^{-1} \equiv (r_N/R)^{-1}$) measured at the end of the experiment. Here, γ_{lg} is the surface tension of water, and r_N is the radius of the neck. The critical stress increases with decreasing radius suggesting that thinner fibers are tougher—an observation in line with that of Griffith's for glass fibers. However, for neck diameters between 270–530 μm ($10^{-3} > \bar{r}_N^{-1} > 6 \times 10^{-4}$), and irrespective of the volume of the initial dispersion or the gap between the plates, the fiber did not break. Instead, the fiber de-bonded from one of the plates. For very small diameters, the liquid bridge was either unstable or the neck would break at very low tensile stresses. Colloidal fibers are extremely delicate at such small diameters and are susceptible to small mechanical vibrations in the rheometer. Fig. 3(a) also includes a few rare cases where debonding was observed for $\bar{r}_N^{-1} < 3 \times 10^{-4}$.

A recent study¹¹ has considered a two dimensional packed bed of colloidal particles that is uni-axially stressed by capillary pressure and determined the stress field close to an elliptical flaw embedded in the packing. In the absence of a flaw, a nonlinear constitutive relation¹² that relates the macroscopic stress in a packed bed saturated with solvent to the macroscopic strain, results in a far-field uniaxial stress that varies as square of the strain. The stress and strain fields are linearized about the pre-crack state to determine the disturbance displacement field immediately after the opening of a mode-I crack. Next, the stress intensity factor for the two dimensional elastic field is related to the surface energy using the Griffith's energy criterion for equilibrium cracks. The calculations show that the dimensionless critical capillary pressure required to open a crack varies inversely with the crack length to the two thirds' power and depends on a dimensionless parameter that measures the ratio of the elastic to surface energy. The following simple scaling analysis¹³ reveals the essence of the results. Since the non-linear constitutive relation suggests a far-field stress that scales with the square of the strain (ϵ^2),

$\sigma \sim E\epsilon^2$, the elastic energy recovered on opening a crack of length $2a$ in a packing of unit thickness scales as, $\sigma\epsilon^2 a^2$. This is because the region of relaxation extends a distance that scales with a from the crack. Here, $E \equiv GM\phi_{rcp}$ is the effective modulus of the packing, G is the shear modulus of the particles, M is the number of nearest neighbors in the packing, and ϕ_{rcp} is the close packing concentration. Equating this to surface energy (γa), gives the critical tensile stress for an equilibrium flaw, $\sigma_c a^{2/3} \sim E^{1/3} \gamma^{2/3}$. It is important to note that the critical stress is independent of the dimensions of the particles in the colloidal packing though the capillary stress (γ_{lg}/R) that exerts the tensile stress will be dependent on the particle size.⁷

Following Sarkar and Tirumkudulu,¹¹ the expression for the critical tensile stress that accounts for the breaking of particle contacts (low pH case) is given by,

$$\left(\frac{\sigma_c R}{2\gamma_{lg}}\right) \left(\frac{a}{R}\right)^{2/3} = A \left(\frac{\phi_{rcp} \gamma_{sg}}{\gamma_{lg}}\right)^{2/3} \left(\frac{GM\phi_{rcp} R}{2\gamma_{lg}}\right)^{1/3}, \quad (1)$$

where $A = 0.45$ for a plane stress deformation, and γ_{sg} is the surface tension of alumina.¹⁴ Since $\gamma_{sg} \gg \gamma_{lg}$, the surface energy contribution from breaking particle contacts, $(\phi_{rcp} \gamma_{sg})$, is much larger than that due to surface tension of the solvent, $((1 - \phi_{rcp})\gamma_{lg})$, and therefore the latter is ignored in (1). Given that the mode-I stress intensity factor for a flaw in a linear elastic two dimensional material and that for a circular flaw of the same dimension embedded in a three dimensional body have identical scaling (with flaw size) and differ only by a factor of order one, $(2/\pi)$,¹⁵ we shall apply (1) to predict the critical stress for our experiments.

Fig. 3(a) plots the predicted dimensionless critical tensile stress (1) as a function of the dimensionless inverse flaw size (\bar{a}^{-1}). Clearly, the measured critical stress follows the same scaling with the neck radius as that with the flaw size. If we assume that the average flaw size is a linear function of the neck radius, $\bar{r}_N \sim 8.6\bar{a}$, then the predicted critical stress (dotted line in Fig. 3(a)) matches well with the experiments, suggesting that the flaw size is constrained by the dimensions of the neck and that the flaw size varies in proportion to the diameter of the neck. Scanning Electron Microscopy (SEM) images revealed voids in failed sections of fibers with neck diameters greater than 700 μm ($\bar{r}_N^{-1} < 5 \times 10^{-4}$) though they were not as frequent in smaller fibers. Of the 10 samples investigated, all the 7 large diameter fibers showed voids while no voids were observed in the thin fibers. Further, the average ratio of neck radius to largest visible void radius was 5.8 (Fig. 3(b)), about the same order as that predicted by theory. This suggests that while the trapped voids were responsible for nucleating cracks in large fibers, packing faults may be the cause for cracks in smaller fibers. The latter, however, could not be confirmed using SEM imaging. Below a critical neck radius, denoted by the vertical dotted line in Fig. 3(a), the colloidal fibers never failed but instead the entire fiber de-bonded from the top plate. The corresponding value of the dimensionless critical stress is 3.8 which sets the stress beyond which the de-bonding occurs. Since the tensile stress is related linearly to the capillary pressure,¹¹ $-\bar{P}_c = \frac{3}{2}\bar{\sigma}_c$, the critical capillary pressure is 5.7. This value is close to the theoretical maximum capillary pressure¹⁶ ~ 5.3 . These results suggest that the maximum allowable tensile stress is set by the maximum capillary pressure which determines the ultimate strength of the colloidal packing. Thus, the region above the horizontal dotted line for $\bar{\sigma}_c > \bar{\sigma}_{\text{max}} = 3.8$ pertains to the unattainable region since the tensile stresses cannot exceed that value implying that if $\bar{r}_N < \bar{r}_{N,c}$ (region to the right of the vertical dashed line

in Fig. 3), then fiber can never crack under capillary stress. Consequently, a packing with large and hard particles can withstand large flaws without failing. These predictions are borne out by the experiments notwithstanding the small scatter in the data. Interestingly, once $\bar{a} < \bar{a}_c$ in the neck region, the entire fiber remains crack-free even though the size of the flaws in other sections of the packing are larger than a_c . This is because, for a given tensile force exerted by the top plate, the local tensile stress at each section of the fiber varies as $\sigma \sim r^{-2}$ and these points lie below the critical tensile stress that varies as $r_N^{-\frac{2}{3}}$. This however assumes that the ratio of the void size to the local fiber diameter remains same everywhere.

While the observations follow the predictions of the aforementioned constitutive relation,¹² we note that the constitutive relation proposed recently by Russel *et al.*⁶ based on the more accurate Hertzian contact mechanics gives a slightly different scaling of critical stress on the flaw size, $\sigma_c \sim a^{-3/5}$. Given the scatter in the data in Fig. 3 (a), the predictions from the two constitutive relations fit the data equally well.

Our study reveals that the critical stress for failure in drying colloidal systems scales differently with flaw size ($\sigma_c \sim a^{-2/3}$) compared to that for brittle materials ($\sigma_c \sim a^{-1/2}$). As in the case of brittle materials, the result is universal and does not depend on the geometry of the colloidal sample. Further, unlike the case of brittle materials, there is a limit to the drying induced tensile stress that is set by the particle size and interfacial tension. Consequently, it is possible to achieve crack-free colloidal packings even in the presence of flaws as long as the critical stress for driving a crack from the flaw is higher than the maximum possible tensile stress. These results are supported by extensive tensile force experiments and evaluation of failed sections using an SEM. The drying dynamics of the liquid bridge and subsequent formation of flaws is a complex process though the shape evolution clearly suggests that the particles first pack close to the top

and bottom plates and the packed front moves towards the middle section. Though detailed calculations are required to elucidate the mechanism for the formation of voids, the experiments clearly show that if the flaw size can be restricted below the critical value predicted by (1), large colloidal packings free of cracks can be synthesized. These results have particular implications for the use of drying techniques to assemble large colloidal packings such as photonic band gap crystals.

The research was financially supported in part by the Department of Science and Technology, India (Project #07DS032). A. S. acknowledges IIT Bombay's support for teaching assistantship.

References

- 1 J. L. Keddie, *Mater. Sci. Eng., R*, 1997, **21**, 101.
- 2 W. B. Russel, *AIChE J.*, 2011, **57**, 1378.
- 3 R. C. Chiu and M. J. Cima, *J. Am. Ceram. Soc.*, 1993, **76**, 2769.
- 4 M. S. Tirumkudulu and W. B. Russel, *Langmuir*, 2005, **21**, 4938.
- 5 C. Petersen, C. Heldmann and D. Johannsmann, *Langmuir*, 1999, **15**, 7745.
- 6 W. B. Russel, N. Wu and W. Man, *Langmuir*, 2008, **24**, 1721.
- 7 W. Man and W. B. Russel, *Phys. Rev. Lett.*, 2008, **100**, 198302.
- 8 A. A. Griffith, *Philos. Trans. R. Soc. London, Ser. A*, 1921, **221**, 163.
- 9 C. E. Inglis, *Proc. Inst. Naval Arch.*, 1913, **55**, 219.
- 10 K. B. Singh, L. R. Bhosale and M. S. Tirumkudulu, *Langmuir*, 2009, **25**, 4284.
- 11 A. Sarkar and M. S. Tirumkudulu, *Phys. Rev. E: Stat., Nonlinear, Soft Matter Phys.*, 2011, **83**, 051401.
- 12 A. F. Routh and W. B. Russel, *Langmuir*, 1999, **15**, 7762.
- 13 K. B. Singh and M. S. Tirumkudulu, *Phys. Rev. Lett.*, 2007, **98**, 218302.
- 14 R. H. R. Castro, S. V. Ushakov, L. Gengembre, D. Gouve and A. Navrotsky, *Chem. Mater.*, 2006, **18**, 1867.
- 15 H. Tada, P. C. Paris, and G. R. Irwin, *The Stress Analysis of Cracks Handbook* (American Society of Mechanical Engineers, 2000).
- 16 G. Mason and D. W. Mellor, *J. Colloid Interface Sci.*, 1995, **176**, 214.